MULTI-SOURCES DATA CORRELATOR PROJECT

Robert Arthur(1), **Miguel Santos**(1), **Gianmario Merisio**(1), **Chiara Manfletti**(1), **Jussi Markkanen**(2), **Thomas Ulich**(2), **Matteo Losacco**(3), **and Jan Siminski**(3)

(1)*Neuraspace, Coimbra, Portugal, Emails: {rob.arthur, miguel.santos, gianmario.merisio, chiara.manfletti}@neuraspace.com*
(2)*EISCAT, Kiruna, Sweden, Emails: {jussi, thomas}@eiscat.se*
(3)*ESA/ESOC, Darmstadt, Germany, Emails: matteo.losacco@ext.esa.int, jan.siminski@esa.int*

ABSTRACT

The space object population is rapidly growing and with that, the pressing necessity of orbit determination for space traffic management and spacecraft operations. In the context of a diverse and fragmented panorama of commercial sensor data, this work describes a prototype service to be integrated into a commercial space traffic management platform and capable of ingesting data from various ground-based sensors and performing accurate orbit determination. To test and validate the prototype, a tracking campaign was conducted during the summer of 2023 on several low Earth orbit objects and an experiment was performed in the first half of 2024 in cooperation with EISCAT using the ultra-high frequency radar in Tromsø, Norway. Results show that both campaigns were successful in tracking and performing orbit determination on the objects. The analysis relied on different sources of precise orbital ephemerides used as ground truth.

Keywords: Low Earth Orbit (LEO), Space Domain Awareness (SDA), Space Situational Awareness (SSA), Space Traffic Management (STM), Orbit Determination (OD), Optical Telescope, Radar.

1. INTRODUCTION

With the current rapid growth in the space object population, accurate orbit determination (OD) for the purposes of space traffic management (STM) and safe and efficient spacecraft operations is becoming ever more critical [1, 2]. The range of commercially available ground-based sensor data is diverse and fragmented, and any commercial STM service would likely have to work with data from various sources and sensor types. In this context, this paper presents a description of the Multi-Source Data Correlator (MSDC) project carried out by Neuraspace in conjunction with ESA's Space Debris Office. The objective was to produce a prototype service that could ingest data from various ground-based sensors and perform accurate OD, with a view to integration in a commercial STM service. The project was conducted under the General Support Technology Programme (GSTP).

The paper breaks down into three parts. It starts with an outline of the tracking data obtained for the project. Then, a description of the software architecture and design choices follows. Eventually, the summary of the results obtained and a discussion about the future developments that will build on the work done under this project are provided.

Since Neuraspace's optical telescopes were not available at the time, optical telescope data was provided by Deimos [3], using an earlier generation of sensors compared to the one now installed by Neuraspace in Portugal and Chile[1], the latter shown in Figure 1. A tracking campaign was conducted during the summer of 2023 on a number of Low Earth orbit (LEO) objects. DiGOS facilitated the provision of laser-ranging data for debris objects [4]. Laser data is also available via the International Laser Ranging Service (ILRS)[2] for various calibration targets and was included in the testing dataset.

Due to the limited commercial availability of radar data, an experiment was conducted in cooperation with EISCAT using the ultra-high frequency (UHF) radar in Tromsø, Norway [5]. The radar was used over a period of 5 days with a 2-hour tracking period each day. The targets were ILRS calibration objects enabling the accuracy of the resulting OD to be established. The experiment was successful in tracking and performing OD on the objects. The remaining issues and constraints are discussed. Neuraspace looks forward to working with EISCAT again in the future, especially when the next-generation radar systems will be operational. These will allow a much greater degree of operational agility than the existing system, making it much better suited to space domain awareness (SDA) applications.

[1] https://blog.neuraspace.com/neuraspace-installs-its-second-optical-telescope-in-chile-for-global-satellite-tracking-coverage [last visit on Mar 25, 2025].

[2] https://ilrs.gsfc.nasa.gov/ [last visit on Mar 25, 2025].

Proc. 9th European Conference on Space Debris, Bonn, Germany, 1–4 April 2025, published by the ESA Space Debris Office
Editors: S. Lemmens, T. Flohrer & F. Schmitz, (http://conference.sdo.esoc.esa.int, April 2025)

Figure 1: Neuraspace's optical telescope in Chile.

The paper then provides an overview of the architecture, design choices and implementation of the prototype. The discussion covers the data flow of tracks entering the system and also describes Neuraspace's approach to managing multiple sources of data for both sensors and estimated ephemeris. It gives results obtained during testing and validation of the system. The analysis was performed using a combination of precise orbital data from Sentinel missions[3] and high-accuracy predictions from ILRS[4] which were used as ground truth [6]. Both of these data sources are publicly available.

Finally, the next developments are discussed including continuous assessment of prediction accuracy and covariance realism, and integration into Neuraspace's existing STM product to provide responsive OD for safe and efficient spacecraft operations.

2. TRACKING DATA

A key objective for the project was to be able to fuse data from diverse ground-based sensors. To this end, data was obtained from optical tracking telescopes, laser ranging, and radar.

2.1. Optical Telescopes

Optical tracking data was obtained from Deimos, using their tracking telescopes in Ciudad Real, Spain [3]. An observation campaign was conducted over a period of 5 nights during the summer of 2023. In parallel to this project Neuraspace has also procured 2 tracking telescopes, which are updated versions of those used during the observation campaign. We briefly summarise some results from the testing and calibration of these sensors, which represent the next phase of Neuraspace's development.

2.2. Laser Ranging

Laser tracking data utilised during the project came from two sources. The first was an observation campaign performed by DiGOS which included laser ranging of debris objects [4]. The second was the publicly available tracking data obtained by the ILRS which tracks a number of objects for calibration purposes [6].

2.3. Radar

An experimental observation campaign was conducted with EISCAT [5] using the radar at Tromsø, Norway, since radar data has limited commercial availability. This observed a number of objects over 5 days during the summer of 2024. Additional optical tracking data were obtained during this period and the results demonstrate the advantages of using data from multiple sources.

3. SOFTWARE ARCHITECTURE AND DESIGN

The development of OD capabilities as part of the MSDC project was done with a view to integration in Neuraspace's software-as-a-service (SaaS) platform for spacecraft operators. As such the implementation has to fit within Neuraspace's existing Amazon Web Services (AWS) framework, and is required to be scalable and fully automated. The general architecture is event-driven. The complete process, depicted in Figure 2 is broken down into three major steps:

- **Track ingestion** - Includes basic normalisations (e. g., for frames, units).
- **Track correlation** - Checks the indicated correlation of the track with an object from the Neuraspace catalogue.
- **Orbit determination** - Generates a new orbit solution after confirming the correlation of a track.

Neuraspace has a number of existing components which are used as part of the track processing and OD processes implemented for the MSDC. Other than versioning and data lineage, the most relevant are:

- **SpaceObjectsAPI** - Contains details on all space objects, combining data from SATCAT[5] and DIS-

[3] https://browser.dataspace.copernicus.eu/ [last visit on Mar 25, 2025].

[4] https://edc.dgfi.tum.de/pub/slr/cpf_predicts/ [last visit on Mar 25, 2025].

[5] https://www.celestrak.org/satcat/search.php [last visit on Mar 25, 2025].

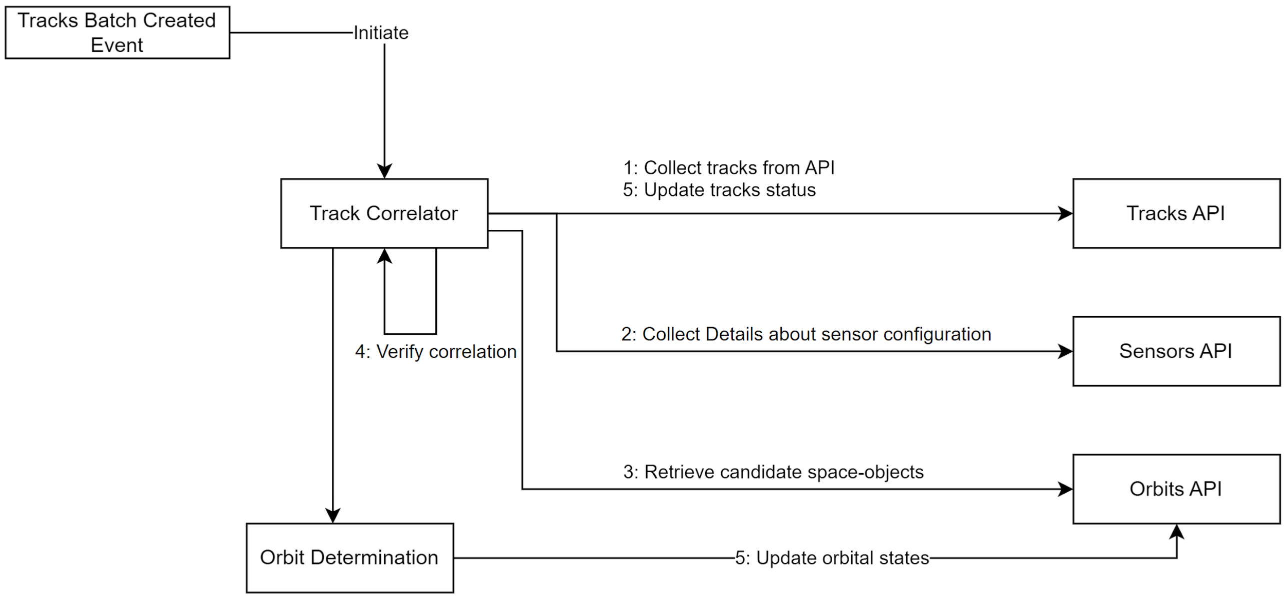

Figure 2: Overall process for track ingestion, track correlation and OD.

COS[6] [7] with that from operators using Neuraspace's platform to ensure object parameters are as accurate as possible.

- **OrbitsAPI** - Stores orbital segments by space object and orbital data series, facilitating the integration of data from multiple sources.

Additional components were built as part of this activity:

- **TracksAPI** - Stores and supplies normalised tracking data.
- **SensorsAPI** - Contains configuration settings on the sensors supplying data to the platform.

3.1. Flight Dynamics Library

For the MSDC-related functionality, Neuraspace selected Orekit[7] as a base library to provide the required flight dynamics functionality. Orekit is a mature software package, with extensive functionality for observation models and OD algorithms [8].

3.2. Track Ingestion

Neuraspace expects to receive data from several sources in the longer term and has therefore designed its data ingestion and storage to be extensible to many types of data. The initial version covers:

- Optical telescope tracks via tracking data messages (TDMs) [9].
- Radar tracks via TDMs [9].
- Laser ranging tracks via consolidated laser ranging data formats (CRDs)[8].

We first parse the file and then apply a normalisation based on the track type before storage. This will convert all units to radians, m or m/s depending on measurement type, and standardise frames where appropriate (e.g., RaDec in EME2000). This simplifies the orbit determination process as all data have already been normalised by the time they reach OD. Ground station configurations can be created and updated. Each configuration has a start date and an optional end date meaning that the correct configuration can be applied to each track individually.

3.3. Track Correlation

The track correlation is the process by which a single track or set of tracks become correlated with a space object, or by which a track's relationship with a space object becomes verified. To establish the correlation, tracks which were already associated with space objects have their association validated, while if this correlation is missed from the track, it will have to be established or a new space object created.

Given the nature of the tracking data obtained, all tracks were pre-correlated and therefore the correlation step implemented acts more as a confirmation of the correlation

[6] https://discosweb.esoc.esa.int/ [last visit on Mar 25, 2025].
[7] https://www.orekit.org/ [last visit on Mar 25, 2025].
[8] https://ilrs.gsfc.nasa.gov/data_and_products/formats/crd.html [last visit on Mar 25, 2025].

Table 1: Summer debris campaign rejection rates.

	No. of different objects	**No. of tracks**	**Median no. of measurements per track**	**Median span** (s)
Deimos (1 telescope)	27	99	140	429
DiGOS (1 SLR station)	9	13	10	147

rather than as a correlation against the entire catalogue. The implementation assesses the normalised residuals vs. synthetic observations generated against the reference ephemeris.

3.4. Orbit Determination

When the OD process is triggered, observations will be gathered for a defined time interval. An appropriate initial state is obtained from the catalogue and a batch least squares (BLS) fit is performed [10, 11].

The BLS method was decided upon for several reasons. Firstly, it is more robust to poor initial states and more resilient to large gaps in data than a sequential estimator. Secondly, it offers the possibility to fit additional parameters such as the drag and SRP coefficients which are crucial for tracking debris where these are unlikely to be available. Thirdly, no process noise tuning is required, so a rough state estimate is enough for initialization. Furthermore, outlier determination is easy (e.g., for incorrectly tagged tracks) and no convergence period and/or monitoring of convergence is required.

There are also obvious shortcomings for the BLS, such as a lack of covariance realism and longer runtime compared to a single-track update for a sequential estimator. Additionally, in the absence of process noise, we still have to deal with uncertainties in state propagation. We can mitigate this disadvantage by using appropriate fit intervals for the orbit, and also by fitting parameters such as drag coefficients, adapting the model to the current conditions. Batch estimators can also make use of consider parameters to represent the uncertainty in unstable parameters such as the drag force [11]. This could be an interesting extension in future.

As mentioned previously, Neuraspace has commissioned its two optical telescopes as a first step in providing automated high-accuracy OD. It intends to add more data sources, both internally and from partners over the coming months and years, but given the small initial data volumes, the BLS algorithm was chosen for simplicity and robustness.

4. RESULTS

We present here the results obtained for the observation campaigns conducted as part of this project. We end with a brief look at the results from the testing and calibration of Neuraspace's two optical tracking telescopes, which took place after the project concluded but is an essential development in providing OD as a reliable service to customers.

4.1. Optical and Laser Debris Tracking Campaign

The summer debris campaign proposes the OD capability demonstration for 30 large targets in LEO orbital regime. Optical and laser ranging measurements are exploited. The former was collected by Deimos' ANTSY telescope and the latter by DiGOS's Borowiec satellite laser ranging (SLR) station. Specifically, the Deimos telescope tracked 27 different objects for a total of 99 tracks, while the DiGOS SLR station tracked 9 different objects for a total of 13 tracks. Overall, observations were carried out for 3 subsequent nights, from 11 to 13 August 2023. A summary of the summer debris campaign in number is presented in Table 1.

Out of the 30 debris targets, 22 were successfully processed while others were filtered from this analysis because of the small amount of passes acquired. Objects with less than 3 pass acquisitions during the campaign were excluded. Their average residuals computed from optical (i.e., RaDec angles) and laser ranging measurements are presented in Figure 3. The reduced chi-squared metric χ^2_ν is reported as well. In the figure, debris are identified by their NORAD ID, which is reported on the x-axis. Additional observation statistics are plotted in Figure 4. On the left y-axis (in red), the number of processed angular and ranging measurements for each debris are reported, while the number of passes per space object is plotted on the right y-axis in blue. Rejection rates for measurements are collected in Table 2.

4.2. EISCAT Radar Tracking Campaign

As part of the EISCAT experiment campaign, five targets have been selected to be tracked: CryoSat 2 (NORAD 36508), Hai Yang 2D (NORAD 48621), Sentinel-3A (NORAD 41335), Sentinel-3B (NORAD 43437), and

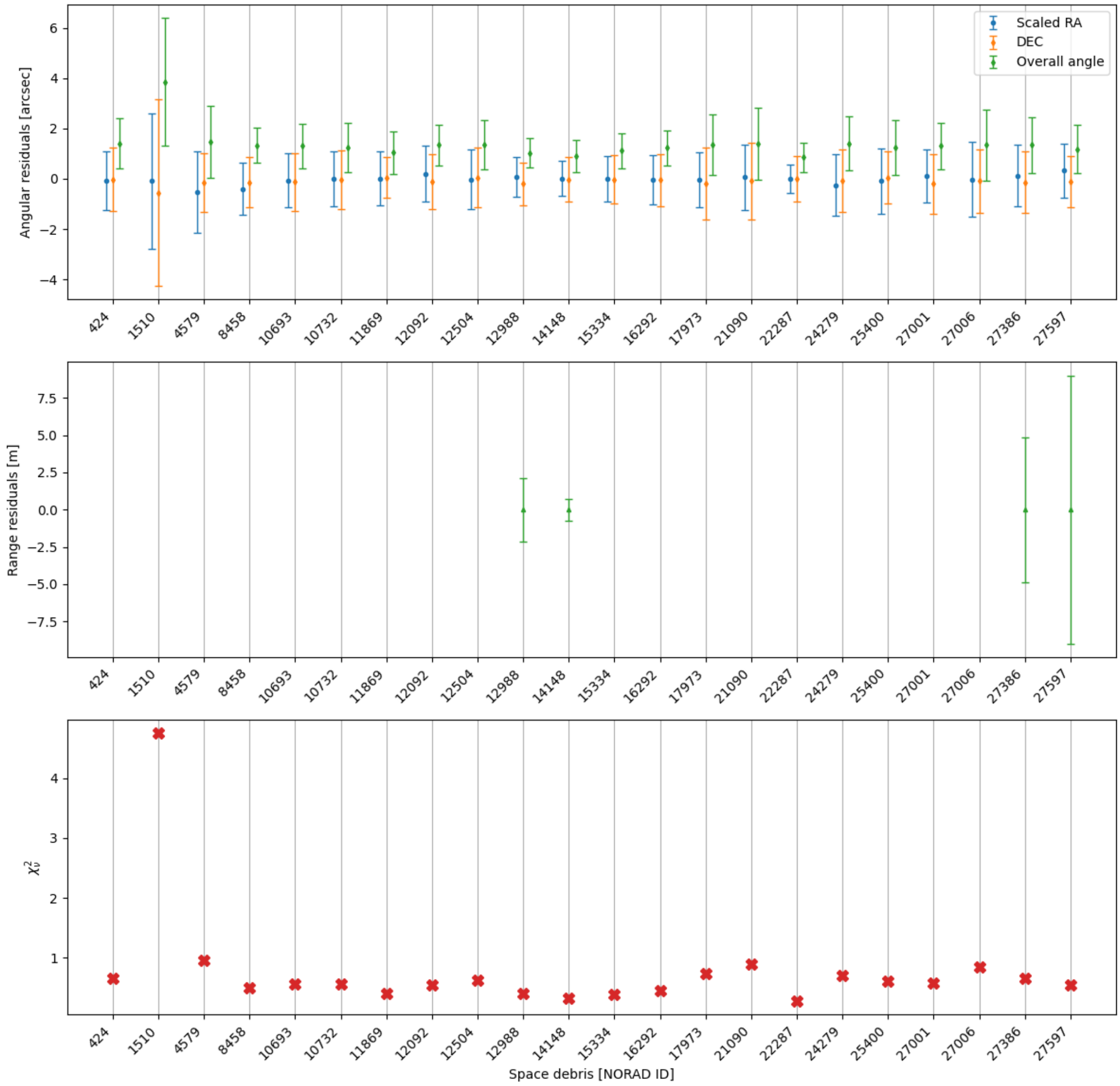

Figure 3: Average residuals for the summer debris campaign. *Top*: Angular RaDec residuals. *Middle*: Range residuals. *Bottom*: Reduced chi-squared statistics χ^2_ν.

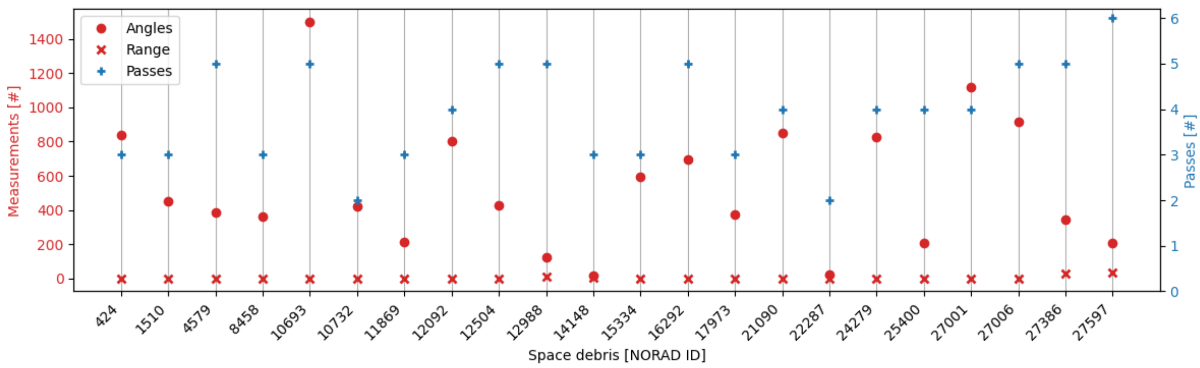

Figure 4: Observation statistics for the summer debris campaign. *Left y-axis*: Number of processed angular (red dot) and range (red cross) measurements. *Right y-axis*: Number of passes (blue plus).

Table 2: Summer debris campaign rejection rates.

NORAD ID	Rejection Rates	
	RaDec	Range
424	0.00%	-
1510	0.22%	-
4579	0.26%	-
8458	0.00%	-
10693	0.00%	-
10732	0.00%	-
11869	0.00%	-
12092	0.00%	-
12504	0.00%	-
12988	0.00%	0.00%
14148	0.00%	0.00%
15334	0.17%	-
16292	0.00%	-
17973	0.27%	-
21090	0.12%	-
22287	0.00%	-
24279	0.24%	-
25400	0.00%	-
27001	0.00%	-
27006	0.43%	-
27386	0.29%	0.00%
27597	0.00%	0.00%

Stella (NORAD 22824). The experiment lasted 5 days, from the 10th to the 14th of June, 2024, with approximately 2 hours of observation per day scheduled to follow the pre-selected targets. The sensor used to perform the observations was the EISCAT's UHF radar [5]. Results for CryoSat 2 and Hai Yang 2D have been omitted because not enough accurate radar measurements were obtained during the observation campaign.

The experiment was executed as follows: *i*) Neuraspace conducted a preliminary analysis to propose EISCAT a list of potential targets and observation slots; *ii*) EISCAT received the list of potential targets and observation slots, reviewed it, and approved it; *iii*) Neuraspace prepared pointing information for all targets within the scheduled observation hours to send before any observation slots (pointings were generated the day before to be more accurate) and shared it with EISCAT. For each target, the pointing information included the most recent TLE and a list of pointing data, each structured to contain the epoch, the azimuth, the elevation, the range, and the pointing duration; *iv*) EISCAT performed the radar observation and sent the obtained measurements to Neuraspace; *v*) Neuraspace produced OD solutions.

Regarding the preliminary analysis to select the targets and observation slots (i. e., step *i*), it was verified that the

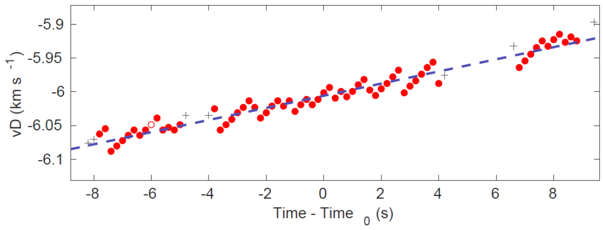

Figure 5: Example produced by EISCAT of range rate measurement during a pass.

shortlisted targets were visible and that the radar could track them fast enough to detect them (max 90 deg/min). About the pointing information (i. e., step *iii*), for each object under consideration, relevant pass data were obtained from TLE. Pass data included a series of planned points to track the spacecraft. The radar followed a multiple beam park approach, so the purpose was to provide directions for the radar to point at while taking into account the time to traverse between points, the movement of the target, the field of view, and potential errors in positions and timings. During processing (i. e., step *v*), Neuraspace discarded measurements with a low signal-to-noise ratio $\sqrt{\mathrm{ENR}} < 30$. The limit was determined experimentally and was seen to improve fits compared to lower values.

The following remarks apply to all the OD solutions presented in this section. Firstly, the altitude location of the EISCAT's UHF radar is accurate to 10s of meters. Secondly, range rate measurements are not very accurate (see Figure 5), as a consequence, only a slight improvement is observed in OD solutions when range rate measurements are considered in estimating the orbit. Next, the time tagging of range and range rate measurements is precise to 1 ms level, which may account for errors in OD solutions in the order of 10 m. An additional 1 s of bias (caused by an accidentally delayed start-up of the radar's microsecond precision timekeeping device) in all measurement epochs was observed and accounted for in producing OD solutions. Finally, by inspecting range and range rate residuals, measurements seem affected by phase ambiguity, see Figure 6. Indeed, range residuals appear to follow the same trend but on different levels, see Figure 6c. By solving such phase ambiguity, the accuracy of the computed OD solutions is expected to improve dramatically.

Data fusion of radar measurements with optical observations was performed to test the OD pipeline. Specifically, a set of telescopic observations was obtained from a commercial provider and fused with EISCAT's radar measurements with the final goal of improving the overall OD solution accuracy. Unfortunately, for these optical sensors, it was not possible to calibrate time biases and sensor accuracies, only a few measurements were collected, and the communicated locations of telescopes were not accurate enough (up to 200 m error in position).

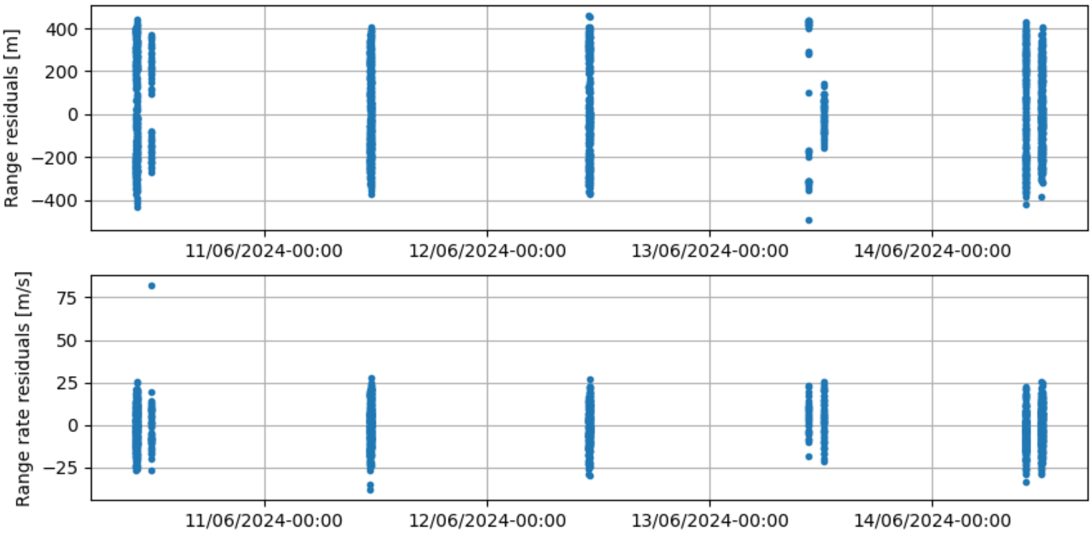

(a) Full residuals collection.

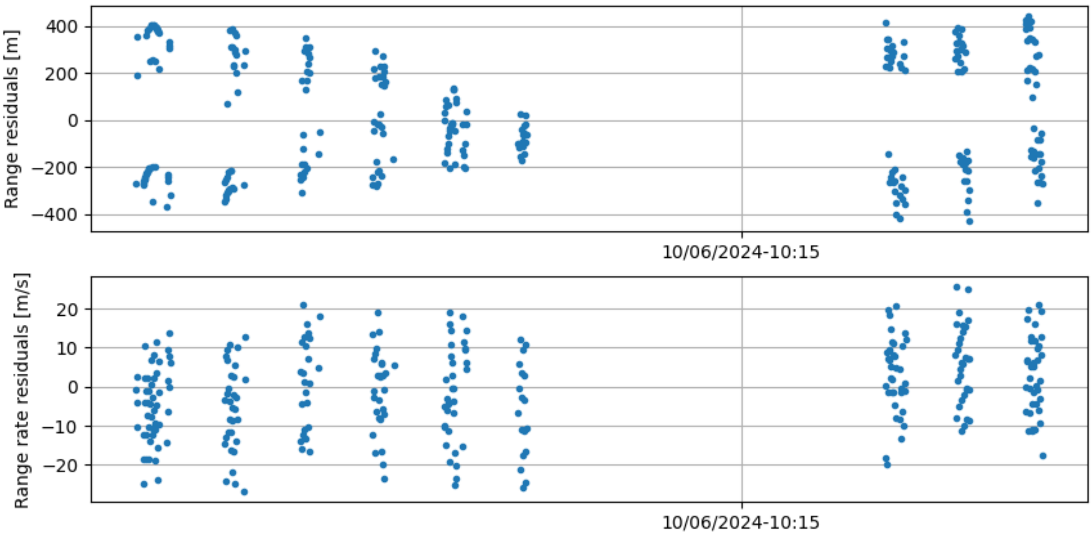

(b) First pass residuals.

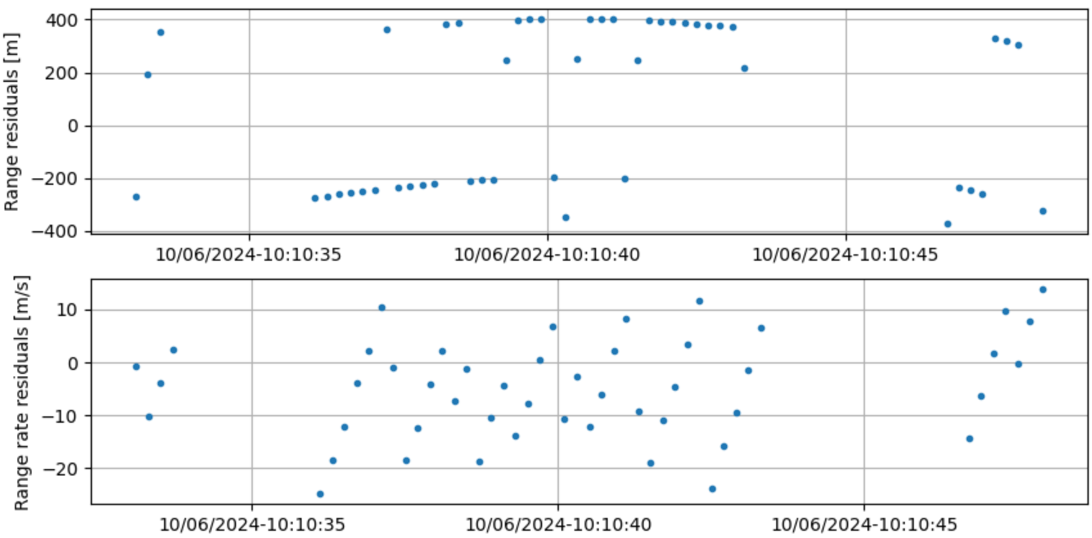

(c) Magnification of first 50 residuals. Possible phase ambiguity on range residuals.

Table 3: Relevant metrics for Sentinel-3A OD products.

EISCAT's radar meas.	
No. of measurements	3354 used out of 3358
Reduced chi-squared χ^2_ν	8.2
Position error Δr **range**	[65, 295] m
Velocity error Δv **range**	[0.069, 0.224] m/s
EISCAT's radar & optical meas.	
No. of measurements	3514 used out of 3568
Reduced chi-squared χ^2_ν	8.1
Position error Δr **range**	[32, 332] m
Velocity error Δv **range**	[0.129, 0.312] m/s
Optical meas.	
No. of measurements	160 used out of 210
Reduced chi-squared χ^2_ν	6.3
Position error Δr **range**	[84, 317] m
Velocity error Δv **range**	[0.040, 0.233] m/s

Table 4: Relevant metrics for Sentinel-3B OD products.

EISCAT's radar meas.	
No. of measurements	2966 used out of 2968
Reduced chi-squared χ^2_ν	10.0
Position error Δr **range**	[81, 218] m
Velocity error Δv **range**	[0.066, 0.153] m/s
EISCAT's radar & optical meas.	
No. of measurements	3149 used out of 3180
Reduced chi-squared χ^2_ν	10.4
Position error Δr **range**	[28, 199] m
Velocity error Δv **range**	[0.017, 0.198] m/s

4.2.1. Sentinel-3A (NORAD 41335) OD Products

The position error for Sentinel-3A over approximately 1 revolution period after the last measurement epoch is shown in Figure 7a. Out of the 3358 range and range rate measurements, 3354 were not rejected by the outlier filter and have been used to produce the OD solution (see Table 3). Data fusion with optical measurements has been performed. The position error of the resulting OD solution is shown in Figure 7b, while additional metrics are provided in Table 3. According to the results, the minimum and maximum errors decreased and increased, respectively. This is actually a slight improvement considering the poor OD solution that is obtained by only using optical measurements (see Figure 7c and Table 3). Indeed, a priori and without a precise Earth observation file (EOF)[9] available, it is tough to tell which is the more accurate series of measurements, therefore fused data should be judged against data obtained from poorer sensors rather than those collected using the best systems. Furthermore, fused data shows that the OD solution actually improved at those latitudes where telescope measurements were considered.

4.2.2. Sentinel-3B (NORAD 43437) OD Products

The position error for Sentinel-3B over approximately 1 revolution period after the last measurement epoch is shown in Figure 8a. Out of the 2968 range and range rate measurements, 2966 were not rejected by the outlier filter and have been used to produce the OD solution (see Table 4). Furthermore, data fusion with optical measurements has been performed. The position error of the resulting OD solution is shown in Figure 8b, while additional metrics are provided in Table 4. In this case, an improvement of the OD solution is observed when performing data fusion. Indeed, the minimum and maximum errors decreased and the optical measurements were able to improve the radar-only OD solution. Note that the orientation in space of the orbit (e.g., the direction of the eccentricity vector with respect to sensor locations) may affect the improvement.

4.2.3. Stella (NORAD 22824) OD Products

The position error for Stella over approximately 1 revolution period after the last measurement epoch is shown in Figure 9a. All 1208 range and range rate measurements have been used to produce the OD solution (see Table 5). Furthermore, data fusion with optical measurements has been performed. The position error of the resulting OD solution is shown in Figure 9b, while additional metrics are provided in Table 5. Similarly to one of the previous cases, also for Stella a slight improvement in the OD solution is observed. Indeed, as before, the minimum and maximum errors decreased and increased, respectively. On the other hand, the improvement with respect to the OD solution produced using only optical measurements is considerable (see Figure 9c and Table 5). Considerations similar to those discussed for the Sentinel-3A also apply here.

4.3. Neuraspace Sensors

To evaluate the calibration and performance of our optical sensors in Portugal and Chile, we collected tracks for objects followed by ILRS and their corresponding con-

[9] https://eop-cfi.esa.int/index.php?view=article&id=349:earth-observation-file-format-standard&catid=78 [last visit on Mar 25, 2025].

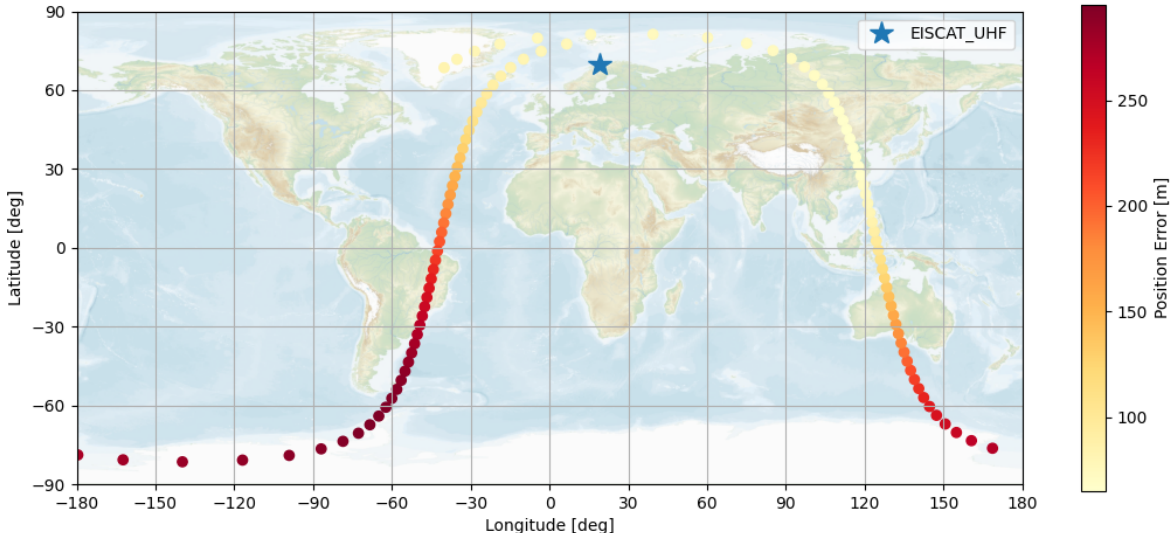

(a) EISCAT data comprising radar measurements from the EISCAT's UHF radar (represented with a star in the plot).

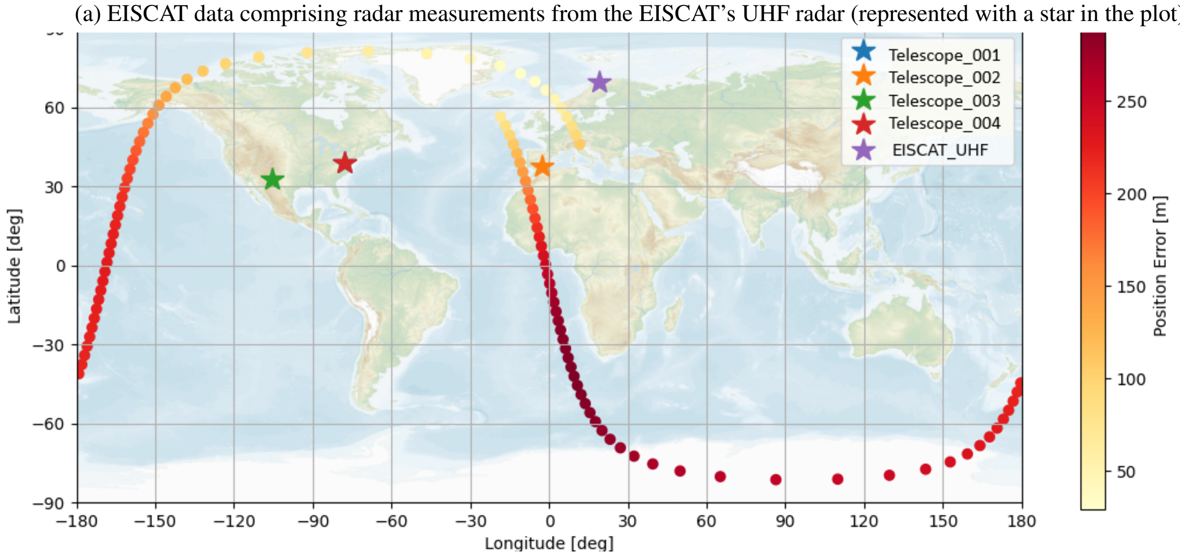

(b) Fusion of EISCAT data comprising radar measurements from the EISCAT's UHF radar (represented with the purple star in the plot) and optical measurements from multiple telescopes (represented with stars in the plot, two stars overlapped).

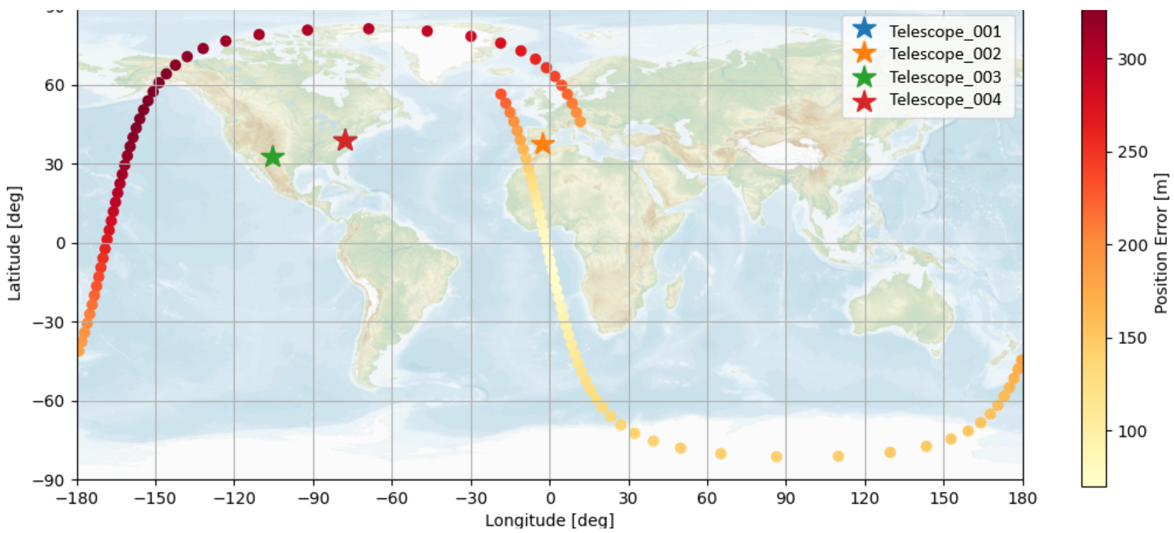

(c) Optical measurements from multiple telescopes (represented with stars in the plot, two stars overlapped).

Figure 7: Position error over the groundtrack of approximately 1 orbit after the last measurement epoch; OD products for Sentinel-3A.

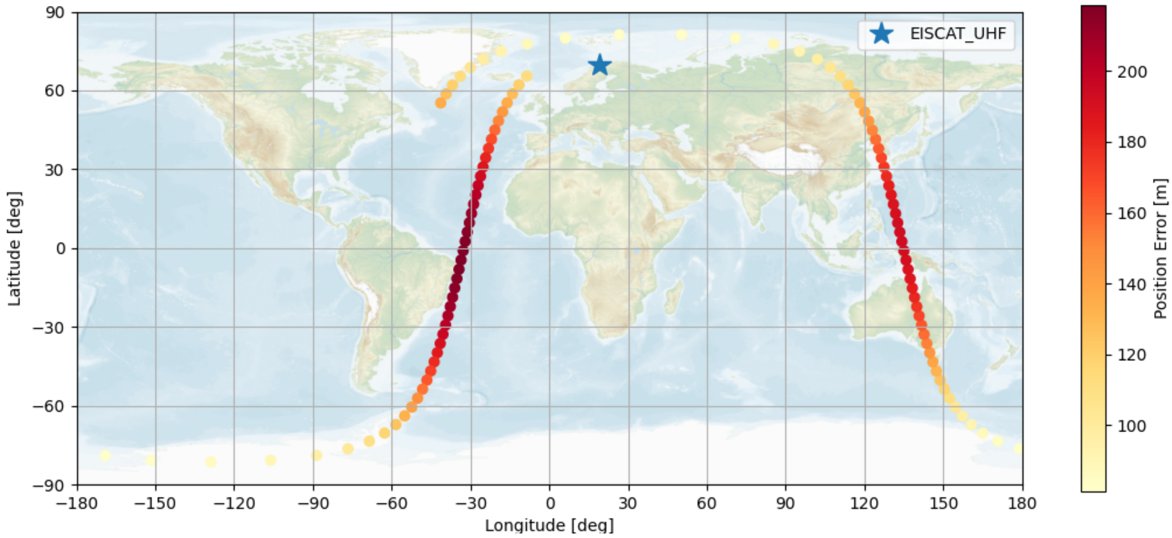

(a) EISCAT data comprising radar measurements from the EISCAT's UHF radar (represented with a star in the plot).

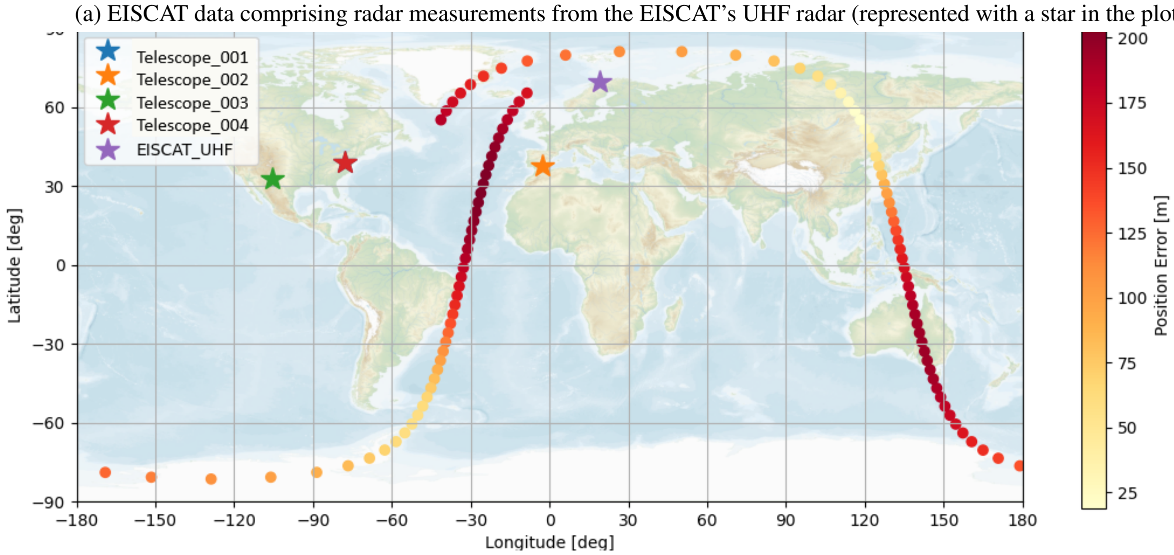

(b) Fusion of EISCAT data comprising radar measurements from the EISCAT's UHF radar (represented with the purple star in the plot) and optical measurements from multiple telescopes (represented with stars in the plot, two stars overlapped).

Figure 8: Position error over the groundtrack of approximately 1 orbit after the last measurement epoch; OD products for Sentinel-3B.

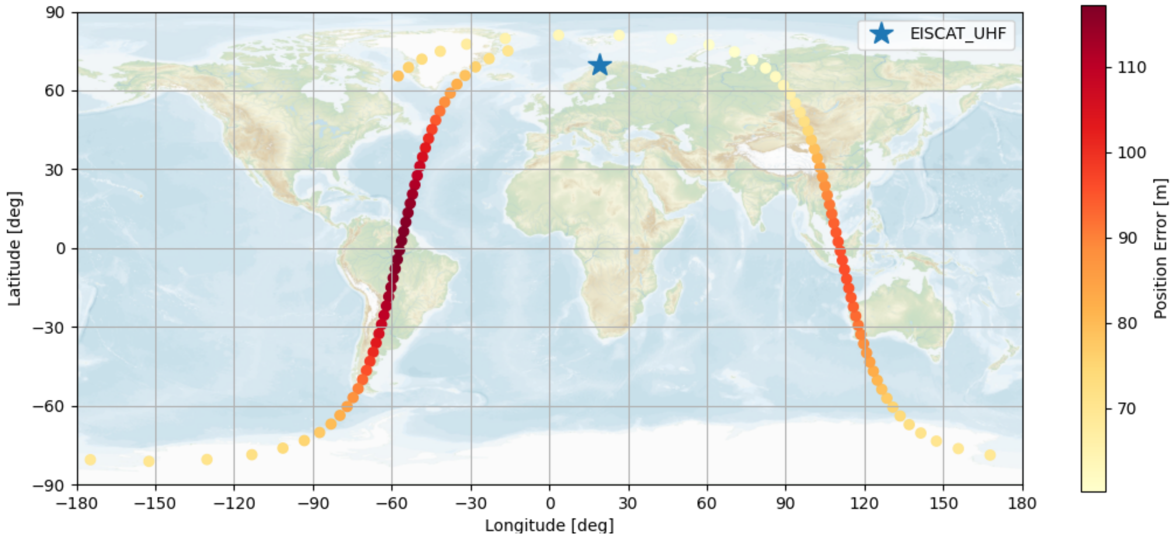

(a) EISCAT data comprising radar measurements from the EISCAT's UHF radar (represented with a star in the plot).

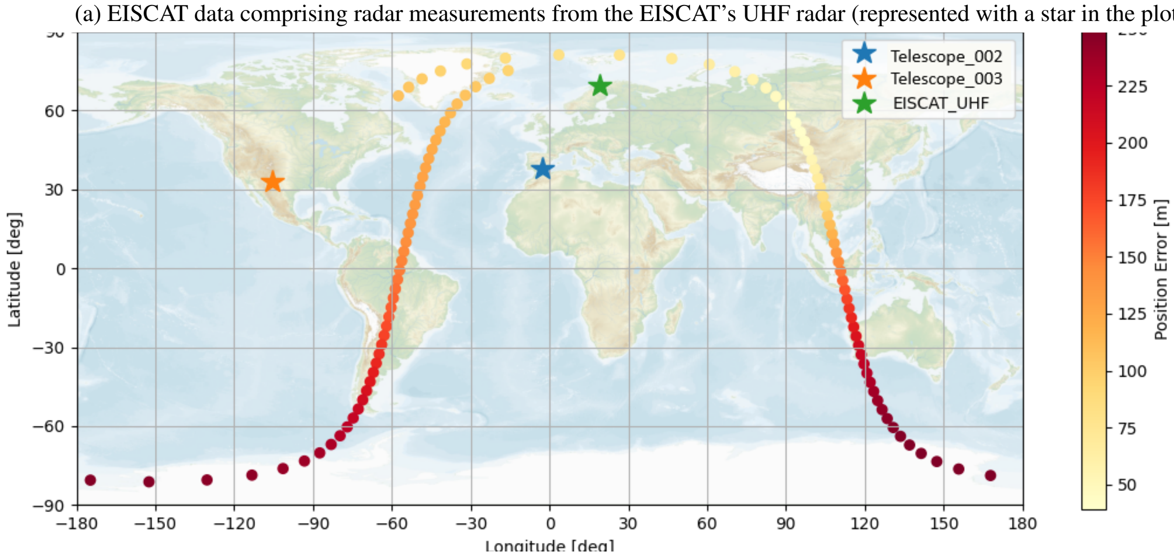

(b) Fusion of EISCAT data comprising radar measurements from the EISCAT's UHF radar (represented with the purple star in the plot) and optical measurements from multiple telescopes (represented with stars in the plot, two stars overlapped).

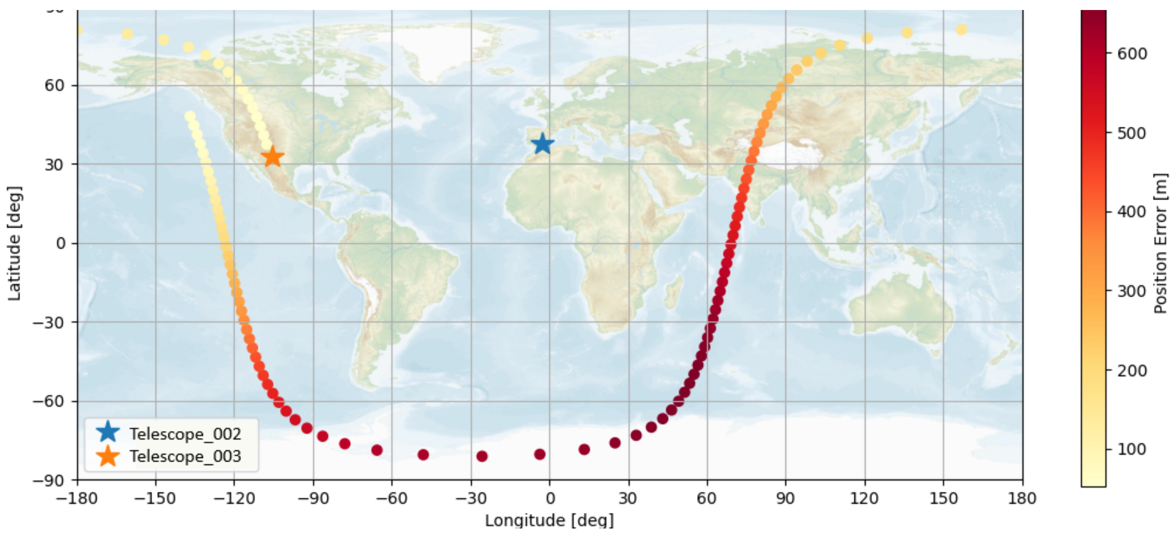

(c) Optical measurements from multiple telescopes (represented with stars in the plot, two stars overlapped).

Figure 9: Position error over the groundtrack of approximately 1 orbit after the last measurement epoch; OD products for Stella.

Table 5: Relevant metrics for Stella OD products.

EISCAT's radar meas.	
No. of measurements	1208 used out of 1208
Reduced chi-squared χ^2_ν	4.4
Position error Δr **range**	[62, 114] m
Velocity error Δv **range**	[0.046, 0.084] m/s
EISCAT's radar & optical meas.	
No. of measurements	1517 used out of 1517
Reduced chi-squared χ^2_ν	3.8
Position error Δr **range**	[39, 252] m
Velocity error Δv **range**	[0.072, 0.207] m/s
Optical meas.	
No. of measurements	309 used out of 309
Reduced chi-squared χ^2_ν	2.0
Position error Δr **range**	[53, 667] m
Velocity error Δv **range**	[0.202, 0.528] m/s

solidated prediction format (CPF) files[10]. To evaluate the performance, we selected three objects with at least 2.5 days of span between the first and last measurements for each sensor. For those space objects, we retrieved the corresponding mass and area from DISCOS. The sensor configuration used assumed an accuracy of 2 arcsec. After gathering all inputs, a batch OD was performed for the whole span of observations by also estimating the drag coefficient when relevant and performing time bias correction. Finally, the OD solution was propagated over one revolution past the last measurement epoch and compared against the ILRS orbit specified in the CPF file.

4.3.1. NOWL Optical Telescope, Portugal

Located in Portugal, the NOWL optical telescope was inaugurated in September 2024. To evaluate its calibration and performance, we selected: Starlette (NORAD 7646), Stella (NORAD 22824), and Hai Yang 2D (NORAD 48621).

According to the results presented in Figure 10 and Table 6, Starlette and Hai Yang 2D have more consistent position and velocity errors, from 18 to 81 m and from 1 to 6 cm/s. On the other hand, STELLA errors are larger, up to 224 m and 20 cm/s. All three targets show good OD quality with low reduced chi-squared values (i. e., 0.3–0.5), indicating potential overfitting. Decreasing the sigma associated with the measurements leads to very similar errors when compared with CPF. Very few observations are rejected during the OD process. Position and velocity errors within one orbital revolution seem to be between 20

[10] https://ilrs.gsfc.nasa.gov/data_and_products/formats/cpf.html [last visit on Mar 25, 2025].

Table 6: NOWL optical telescope performance.

Starlette OD product	
Tracks	4 days span, 7 passes
No. of measurements	822 used out of 822
Reduced chi-squared χ^2_ν	0.3
Drag coefficient c_D	1.1
Position error Δr **range**	[18, 80] m
Velocity error Δv **range**	[0.010, 0.057] m/s
Stella OD product	
Tracks	4 days span, 5 passes
No. of measurements	758 used out of 758
Reduced chi-squared χ^2_ν	0.3
Drag coefficient c_D	2.1
Position error Δr **range**	[14, 224] m
Velocity error Δv **range**	[0.047, 0.171] m/s
Hai Yang 2D OD product	
Tracks	3 days span, 5 passes
No. of measurements	456 used out of 459
Reduced chi-squared χ^2_ν	0.5
Drag coefficient c_D	8.6
Position error Δr **range**	[34, 81] m
Velocity error Δv **range**	[0.026, 0.050] m/s

m and a few cm/s to around 200 m and 10 cm/s. Position errors, in particular the ones at the date of the last measurement, are consistent with typical errors in position prediction of CPF files being of at most a few tens of meters[11]. Finally, results are consistent with Leolabs system metrics[12] which report position differences between their state vectors and the ILRS ones of around 50 m, and position uncertainties of roughly 20 m.

4.3.2. SOWL Optical Telescope, Chile

Located in Chile, the SOWL optical telescope has been operational since December 2024. To evaluate its calibration and performance, we selected: LARES (NORAD 38077), Jason-3 (NORAD 41240), and Sentinel-6 (NORAD 46984).

As shown in Figure 11 and Table 7, all objects have consistent position and velocity errors. The three targets show good OD quality with reduced chi-squared values between 0.3–1.8, so suggesting overfitting which is likely because we maintained a 2 arcsec theoretical sigma for the whole analysis. As for NOWL, also for SOWL only

[11] http://sgf.rgo.ac.uk/qualityc/cpf_qc_resids.html [last visit on Mar 25, 2025].
[12] https://platform.leolabs.space/system_metrics [last visit on Mar 25, 2025].

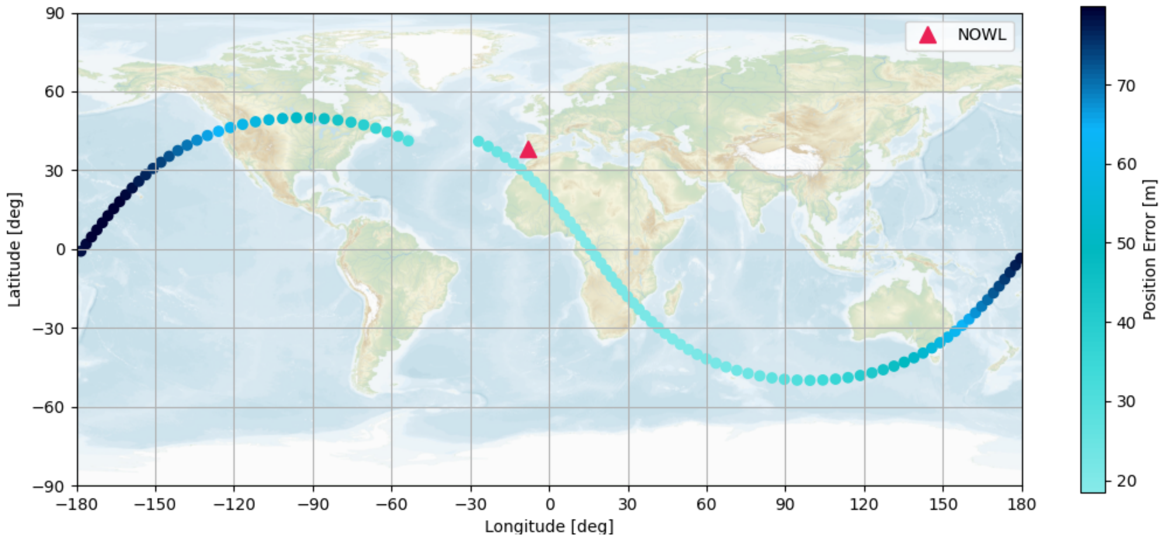

(a) Starlette; 805 km x 1107 km x 49.8 deg.

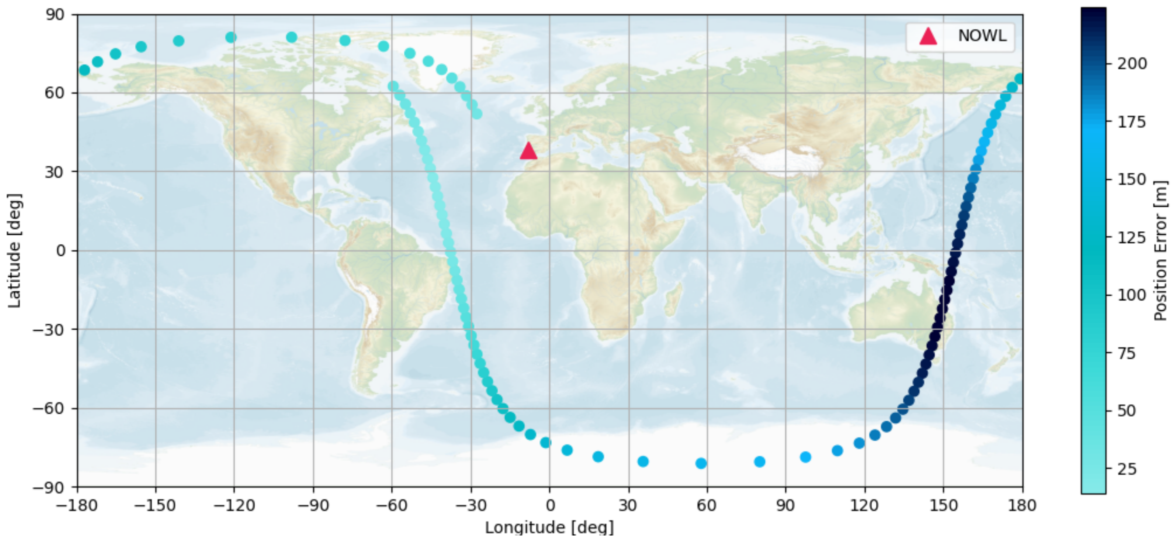

(b) Stella; 795 km x 806 km x 99.9 deg.

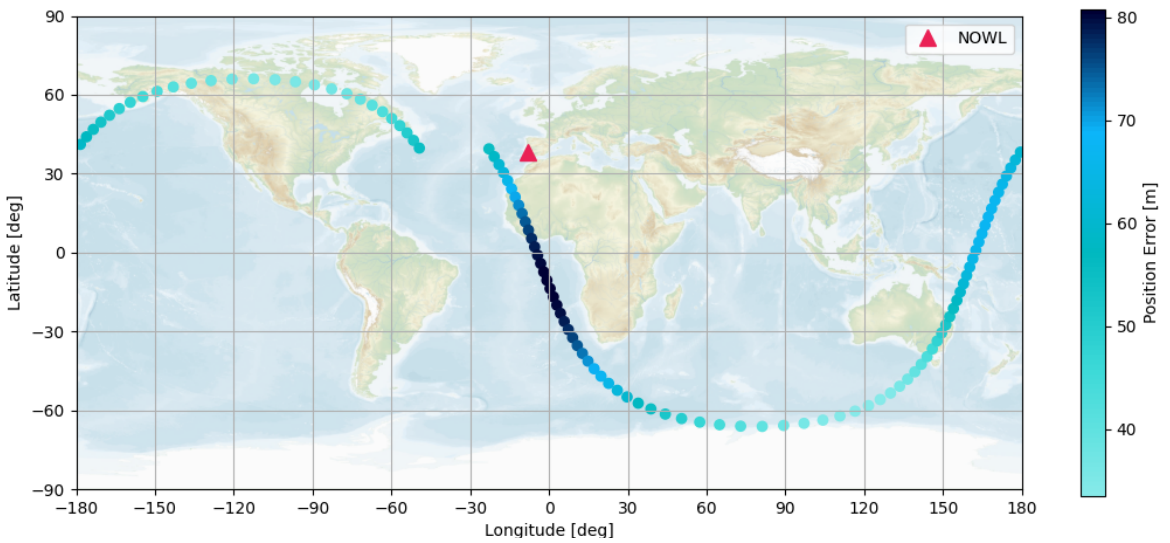

(c) Hai Yang 2D; 945 km x 959 km x 66.0 deg.

Figure 10: OD propagated state vectors from NOWL observations compared against ILRS solutions over one orbital revolution.

Table 7: SOWL optical telescope performance.

LARES OD product	
Tracks	6 days span, 6 passes
No. of measurements	36 used out of 87
Reduced chi-squared χ^2_ν	0.6
Position error Δr **range**	[4, 121] m
Velocity error Δv **range**	[0.040, 0.113] m/s
Jason-3 OD product	
Tracks	7 days span, 9 passes
No. of measurements	116 used out of 116
Reduced chi-squared χ^2_ν	0.4
Position error Δr **range**	[84, 273] m
Velocity error Δv **range**	[0.038, 0.177] m/s
Sentinel-6 OD product	
Tracks	6 days span, 7 passes
No. of measurements	133 used out of 135
Reduced chi-squared χ^2_ν	0.3
Position error Δr **range**	[52, 200] m
Velocity error Δv **range**	[0.012, 0.126] m/s

a few observations were rejected, except for LARES. If compared against the results from the NOWL performance campaign discussed in the previous section, results here were generated with fewer measurements (2 to more than 10 times fewer measurements), but with longer OD spans. Nevertheless, similarly to NOWL, position and velocity errors within one orbital revolution seem to be bounded from 20 m and a few cm/s to around 300 m and 10 cm/s.

5. CONCLUSION

The activity has de-risked the development of an MSDC demonstration model for a commercial STM service. The MSDC has demonstrated the ability to use optical, laser and radar measurements of spacecraft both individually and in combination to provide an accurate OD solution. Key capabilities such as high-accuracy orbit propagation, rapid processing of TDMs and successful handling of asynchronous received data have been validated. This has been done using an architecture compatible with Neuraspace's SaaS platform, paving the way for it to be made available to operators.

Data from laser stations was shown to be fitted to metre-level accuracy, consistent with the size of the spacecraft. An optical telescope very similar to the ones that Neuraspace has now installed in Portugal and Chile demonstrated accuracy. Finally, an experimental radar capability was demonstrated in conjunction with EISCAT. Results were promising although there remain some calibration details to work through. The radar results are particularly exciting as radar does not suffer from the same weather and lighting restrictions that we find with optical telescopes.

With all of these sensors, a primary limitation was shown to be the use of a single ground station and as a consequence an under-determination of the full orbit. This highlights one of the key benefits of data fusion, the ability to take different measurements at several points in the orbit, thus offsetting the weaknesses of the other sensors and improving overall accuracy. This improved accuracy was highlighted in the paper. Overall, the MSDC demonstration model TRL level has been successfully increased from 3 to 7 with demonstration and evaluation of the prototype in an operational environment, so successfully achieving the objective of the project.

Concerning the future, Neuraspace plans to integrate several items to further enhance its OD capabilities:

- A sequential estimator will be added alongside the BLS so that the two techniques can be used in a complementary manner to provide the benefits of both.
- Further extension to include features such as consider parameters may also prove beneficial.
- Enhanced correlation to handle unknown objects and those which may have manoeuvred since the previous OD.
- Pursue the collaboration with EISCAT to operationalise the use of the radar, particularly in relation to next-gen systems.

The quality of OD products when combining measurements from NOWL and SOWL optical telescopes is currently under assessment and will be presented as part of future works. As expected, preliminary results show that using tracking data from both telescopes significantly reduces the maximum errors (up to 7 times). Additionally, Neuraspace's ambition is to bring together the benefits of AI/ML with traditional flight dynamics approaches in order to provide the additional capabilities required for the space environment of the future [2]. As such, we are pursuing AI developments in areas such as atmospheric density prediction [12], pattern of life recognition [13, 14] and anomaly detection which will be relevant to our OD processes.

ACKNOWLEDGMENTS

The work described in this paper has been funded by the European Space Agency under the GSTP, ESA contract No. 4000141190/23/NL/GLC/CB, supported by the national delegation of Portugal. The authors would like to acknowledge the help received by A. Ribeiro and the entire Neuraspace team while working on the project.

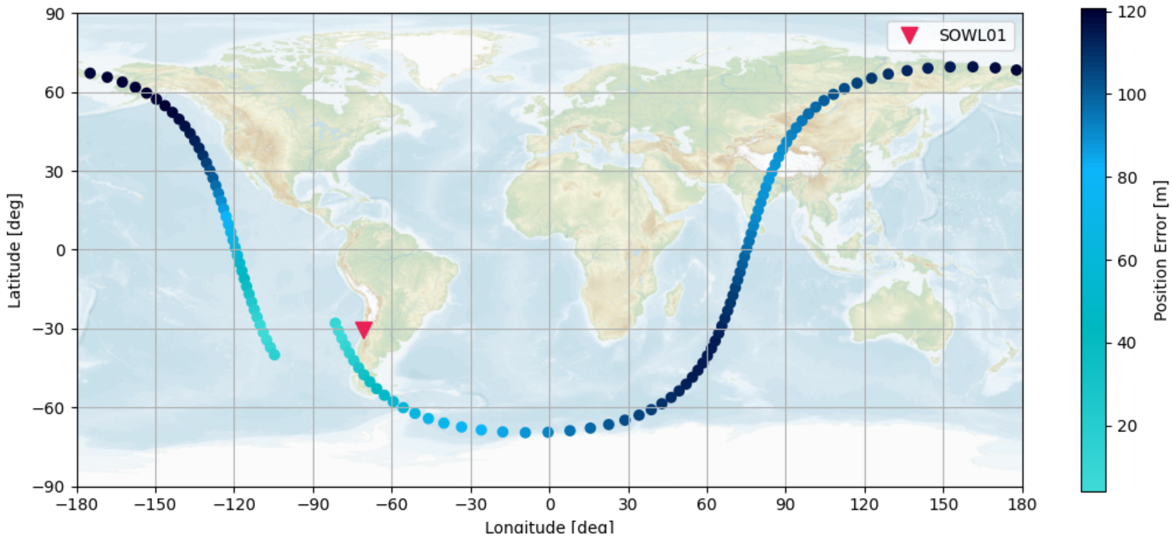

(a) LARES; 1439 km x 1449 km x 69.5 deg.

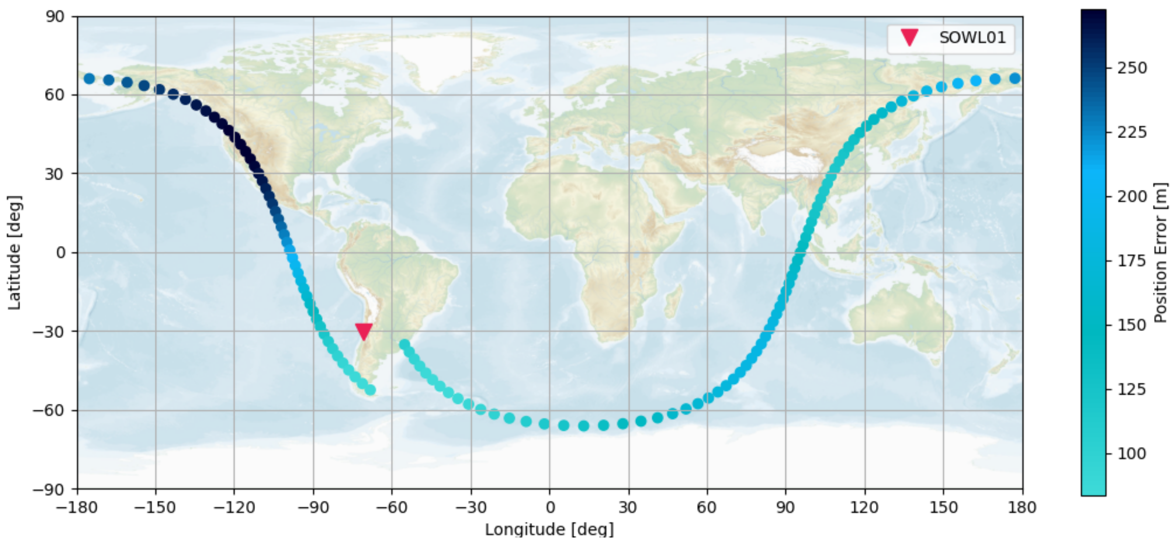

(b) Jason-3; 1331 km x 1344 km x 66.0 deg.

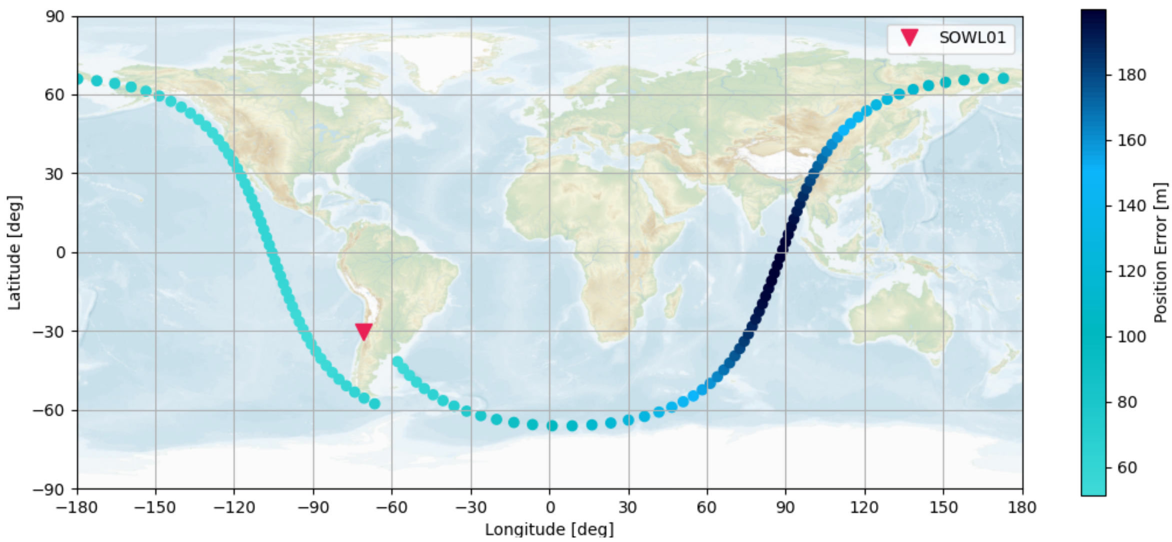

(c) Sentinel-6; 1332 km x 1344 km x 66.0 deg.

Figure 11: OD propagated state vectors from SOWL observations compared against ILRS solutions over one orbital

REFERENCES

1. ESA Space Debris Office, (2024). *ESA's Annual Space Environment Report*.
2. Manfletti C., Guimarães M., and Soares C., (2023). *AI for space traffic management*, Journal of Space Safety Engineering 10.4: 495-504. DOI: 10.1016/j.jsse.2023.08.007
3. Sánchez-Ortiz N., Domınguez-González R., et al., (2021). *Calibration and Analysis of Orbital Accuracy through SST Observations*, 8th European Conference on Space Debris. ESA Space Debris Office.
4. Kloth A., Steinborn J., et al., (2019). *On the horizon: new ESA Laser Ranging Station (ELRS) with debris tracking capabilities*, Proceedings of the 1st NEO and Debris Detection Conference.
5. Baron M., (1984). *The EISCAT facility*, Journal of Atmospheric and Terrestrial Physics 46: 469-472. DOI: 10.1016/0021-9169(84)90065-5
6. Pearlman M.R., et al., (2019). *The ILRS: approaching 20 years and planning for the future*, Journal of Geodesy 93: 2161-2180. DOI: 10.1007/s00190-019-01241-1
7. Flohrer T., et al., (2013). *DISCOS-current status and future developments*, Proceedings of the 6th European Conference on Space Debris. Vol. 723.
8. Maisonobe L., Pommier V., and Parraud P., (2010). *Orekit: An open source library for operational flight dynamics applications*, 4th international conference on astrodynamics tools and techniques. Paris: European Space Agency.
9. CCSDS, (2020), Tracking Data Message – Recommended Standard CCSDS 503.0-B-2.
10. Montenbruck O., Gill E., and Lutze F.H., (2002). *Satellite orbits: models, methods, and applications*, Appl. Mech. Rev. 55.2: B27-B28.
11. Tapley B.D., Schutz B.E., and Born G.H., (2004). *Statistical orbit determination*, Elsevier.
12. Guimarães M., Almeida M., et al., (2024). *Predicting the Thermospheric Density in LEO with Deep Learning*, European Space Weather Week.
13. Guimarães M., Soares C., and Manfletti C., (2024). *Identifying Operational Patterns in LEO Satellite Orbits through Time Series Clustering*, 75th International Astronautical Congress.
14. Guimarães M., Soares C., and Manfletti C., (2024). *Data-Driven Identification of Main Behavioural Classes and Characteristics of Resident Space Objects in Low Earth Orbit through Unsupervised Learning*, Advanced Maui Optical and Space Surveillance Technologies (AMOS) Conference.